Journal of the Meteorological Society of Japan, Vol.79, No.6, pp.1207–1227, 2001

The Seasonal and Intraseasonal Variability of Diurnal Cloud Activity over the Tibetan Plateau

By Hatsuki Fujinami and Tetsuzo Yasunari

Institute of Geoscience, University of Tsukuba, Tsukuba, Japan

(Manuscript received 17 September 1999, in revised form 3 September 2001)

Abstract

Seasonal variation of diurnal cloud activity (abbreviated DCA) over the Tibetan Plateau throughout the year is examined using 3-hourly geostationary meteorological satellite (GMS) data for 6-years (1989–1994). The DCA shows two distinct variance maxima in the seasonal cycle. One is in spring (pre-monsoon season), and the other is in the summer monsoon season. The DCA begins in late January, and reaches its maximum from March through April. The active DCA extends over almost the whole of the plateau, especially over the southern part (around 30°N, 90°E) and the zonally oriented belt between 35°N, 80°E and 31°N, 102°E. A short interval between the two active DCAs is found around late May to early June. The DCA starts again over the southeastern region of the plateau (centered around 30°N, 101°E) in June and moves up to the southern region. From July to August, the DCA is most active over the southern region (around 30°N, 86°E). After September, the active DCA retreats to the southeastern region.

In both spring and summer, the amplitude of the DCA fluctuates on intra-seasonal time scales. In the active period of the DCA in spring, corresponding to the meandering of the upper-level mid-latitude westerly to the south of the plateau with a trough, the cold air mass at the upper-level is clearly seen over the plateau and weak wind speed is observed through the plateau troposphere. This atmospheric structure and a heating of the lower atmosphere during daytime are likely to be responsible for the enhancement of the DCA in spring. In contrast, during summer monsoon season, the increase of humidity and temperature are identified at the lower atmosphere over the plateau, associated with a humid and warm air intrusion from the South Asian monsoon area into the lower atmosphere over the plateau and precipitation due to active convection. This indicates an increase of the instability for moist convection. These features of the atmospheric circulation and the surface heating during daytime induce active moist convection. Corresponding to the enhanced DCA over the southern part of the plateau, the center of the Tibetan high is located over there. A possible mechanism for the intraseasonal variability of the DCA associated with that of the upper-level atmospheric circulation is also discussed.

1. Introduction

The Tibetan Plateau has a large thermal influence as well as a dynamical effect on atmospheric circulation. During the Asian summer monsoon season, thermally-induced direct circulation occurs as a branch of the planetary-scale Asian summer monsoon circulation (Luo and Yanai 1983; Yanai et al. 1992). In addition, the thermal contrast between the Eurasian continent, particularly at the low latitudes, and the adjacent oceans is strengthened by the existence of the plateau. The land-ocean contrast triggers large scale low-level monsoon westerlies (He et al. 1987; Li and Yanai 1996). Recently, Ueda and Yasunari (1998) pointed out that the early onset in mid-May of the Asian summer monsoon over the Bay of Bengal and the South China Sea is likely induced by the thermal contrast between the Tibetan Plateau and the adjacent ocean.

The plateau is a heat source from March to October, and a heat sink from November to Febru-

Corresponding author: Tetsuzo Yasunari, Institute of Geoscience, University of Tsukuba, Ibaraki 305-8571, Japan.
E-mail: yasunari@atm.geo.tsukuba.ac.jp

ary (Yanai et al. 1992; Li and Yanai 1996). Sensible heating from the surface provides a major source of heating in the pre-monsoon season with its maximum value over the western plateau. In the summer rainy season, latent heating by cumulus convection also becomes a major heat source over the eastern plateau (Yeh and Gao 1979; Nitta 1983).

Previous studies found remarkable diurnal variations over the plateau in temperature, humidity, wind speed, convective activity and other meteorological elements (Yeh and Gao 1979; Gao et al. 1981; Murakami 1983; Yanai et al. 1992; Nitta and Sekine 1994; Yanai and Li 1994; Endo 1996). During the GEWEX (Global Energy and Water Cycle Experiment) Asian Monsoon Experiment (GAME), GAME–Tibet IOP (Intensive Observation Period) was conducted to clarify the interactions between the land surface and atmosphere over the Tibetan Plateau from May to September 1998 (Koike et al. 2001). Apparent diurnal variations of convective clouds and precipitation cells were observed by the doppler radar and the precipitation radar (PR) of the Tropical Rainfall Measuring Mission (TRMM) over the central part of the plateau during the IOP (Shimizu et al. 2001; Uyeda et al. 2001). These large diurnal variations are closely associated with the development of the planetary boundary layer over the plateau, indicating that an energy exchange between the boundary layer and the free atmosphere through the diurnal cycle is important to form a general circulation over the plateau and the surrounding regions.

The latent heat released by condensation is a major source of heating to maintain atmospheric general circulation over the monsoon and tropical regions. IR–Tbb (infrared equivalent blackbody temperature) and OLR (Outgoing Longwave Radiation) data derived from meteorological satellites have been used to study cloud activity over these regions. These elements are good measures for convective activity associated with various disturbances. Such convection of clouds contains important information to estimate heating and hydrological processes in the atmosphere. Therefore, analyses based on these satellite-derived data are useful for investigating thermal and dynamic processes in the atmosphere in these regions.

Murakami (1983) examined spatial distributions of diurnal variations of the deep convection over the western Pacific and Southeast Asia during FGGE (First GARP Global Experiment) period based on the convective index Ic derived from GMS (Geostationary Meteorological Satellite)–IR data. He showed that the time of maximum convective activity over land is in late afternoon at around 18 LST, while over adjacent oceanic regions, it is in the morning. Nitta and Sekine (1994) specified spatial distributions of amplitude and phase in the diurnal variations of convection over the tropical western Pacific by using long period GMS–IR data. They also defined the convective index Ic, which differs from that of Murakami (1983), to identify convective activity of cumulus-type and to eliminate the effect of surface temperature. Some studies by these satellite-derived data have also shown that enhanced convective activity occurs over the southern part of the plateau during the Asian summer monsoon (Murakami 1983; Murakami 1984; Nitta and Sekine 1994; Yanai and Li 1994). Murakami and Matsumoto (1994) redefined monsoon domains by the annual difference of OLR. They showed that the southern plateau forms one part of the Asian summer Monsoon domain.

Cloud activity is an important physical process not only for changing the surface heat balance through precipitation, but also for controlling the energy balance through radiative forcing. Some previous studies focused on radiative forcing by snow over the Tibetan Plateau. Yasunari et al. (1991), Vernekar et al. (1995) and Ose (1996) showed that anomalous snow cover over the plateau induces atmospheric cooling by the albedo effect, and delays the establishment of the following summer monsoon. They also pointed out that atmospheric heating is suppressed by snow-hydrological effects especially in early spring. Cloud radiative forcing plays an important role in regulating the heat and energy balance over the Tibetan Plateau. Clouds produce large values of cloud-top longwave cooling and smaller values of shortwave warming within a cloud layer. Below a cloud layer, there is a reduction in longwave cooling because of the cloud-induced greenhouse warming effect as well as a reduction of incoming shortwave radiation because of the enhanced cloud albedo effect. The net effect of clouds is a radiative cooling of the plateau atmosphere during the summer rainy season, because cloud-induced longwave cooling exceeds cloud-induced shortwave heating (Smith and Shi 1995).

However, the seasonal variation of cloud activity over the Tibetan Plateau is not yet fully understood, because in analyses based on IR data, it is

difficult to distinguish low ground surface temperature from cloud-top temperature in winter through early spring. To comprehend the mechanisms of heating and the hydrological cycle over the plateau, further analysis is necessary to clarify the features of cloud activity and the mechanisms of cloud development throughout the year.

The main objectives of the present paper are: 1) to describe the seasonal and regional characteristics of the diurnal cloud activity (hereafter abbreviated to DCA) over the plateau throughout the year based on IR data, and 2) to show the variability of the DCA and structures of associated atmospheric circulation for the active/inactive periods of the DCA at the intraseasonal time scales.

Data and methods of analysis are described in Section 2. Section 3 reveals the spatial characteristics and seasonal changes of the DCA over the plateau. In addition, characteristics of clouds are examined using GMS–Visible images and IR–Tbb data with higher spatial resolution. The seasonal migration of atmospheric static stability is also presented. In Section 4, we detail the intraseasonal variation of the DCA, and the structure of the atmospheric circulation for the active and the inactive periods of the DCA. A possible mechanism for generating the variability in the DCA is then discussed. Summary and remarks are given in Section 5.

2. Data and methods of analysis

3-hourly IR–Tbb data for 6-years (1989–1994) derived from GMS are utilized in this study. Tbb data are obtained at each 1° × 1° grid point. In order to examine the seasonal change of the DCA, the index of cloud activity is defined by considering the difference of the diurnal cycle of Tbb, which includes information about both ground surface temperature and cloud-top temperature.

In order to study the regional characteristics of diurnal cycles of Tbb in detail, we choose two different regions, as shown in Fig. 1. Additionally, to confirm the total cloud activity over the plateau during summer (JJA), the horizontal distribution of convective index Ic presented by Nitta and Sekine (1994) is also illustrated. It is defined by

$$Ic = 250 - Tbb \qquad (Tbb < 250K), \tag{1}$$

$$Ic = 0 \qquad (Tbb \geq 250K). \tag{2}$$

where 250 K corresponds to the air temperature near 9000 m above sea level over the Plateau for

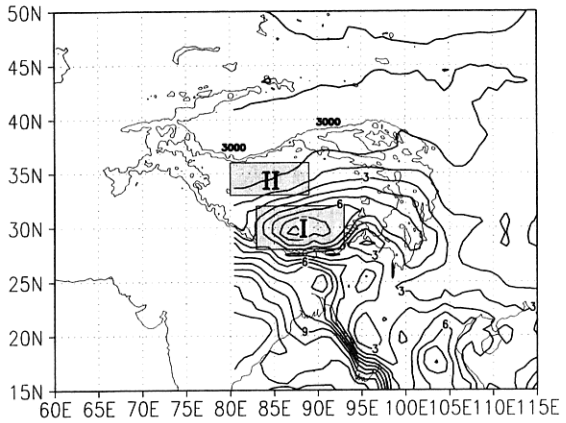

Fig. 1. Geographical map of the Tibetan Plateau (thin solid lines) and the 6-year averaged (1989–94) Ic defined by Nitta and Sekine (1994) for the summer (JJA) (thick solid). Topography is drawn by global gridded elevation and bathymetry (ETOPO5), and topographic contours for 3000 m and 4500 m are shown. The contour interval is 1 for Ic. Boxes I, II represent two regions for the detailed study of cloudiness.

summer (JJA). This Ic thus represents an index for the deep convective clouds whose top height exceeds about 9000 m. In this study, we treat the areas at greater than 3000 m above sea level as the Tibetan Plateau.

Region I (28°–32°N, 83°–93°E) is located in the southern part of the plateau. Active convection with precipitation occurs in this region during the summer monsoon season (Murakami 1983; Nitta and Sekine 1994; Yanai and Li 1994). This region contains the center of enhanced convective activity as shown in Fig. 1. Region II (33°–36°N, 80°–89°E) is located in the western part of the plateau. This region has little annual precipitation and is classified as a desert or dry region (Shi and Smith 1992). It is evident from Fig. 1 that the convective activity over this region is suppressed compared with that over region I.

Figure 2 shows the 6-year averaged monthly diurnal cycles of Tbb for the two regions. The diurnal cycles of Tbb for July and August (Fig. 2-a), corresponding to the summer rainy season over Region I, show a maximum value from 03 to 06 UTC (09–12 LST at 90°E) and a minimum value around 12 UTC (18 LST). Convective activity over the Tibetan Plateau is rapidly enhanced in the afternoon and reaches its maximum at 12 UTC (18 LST)

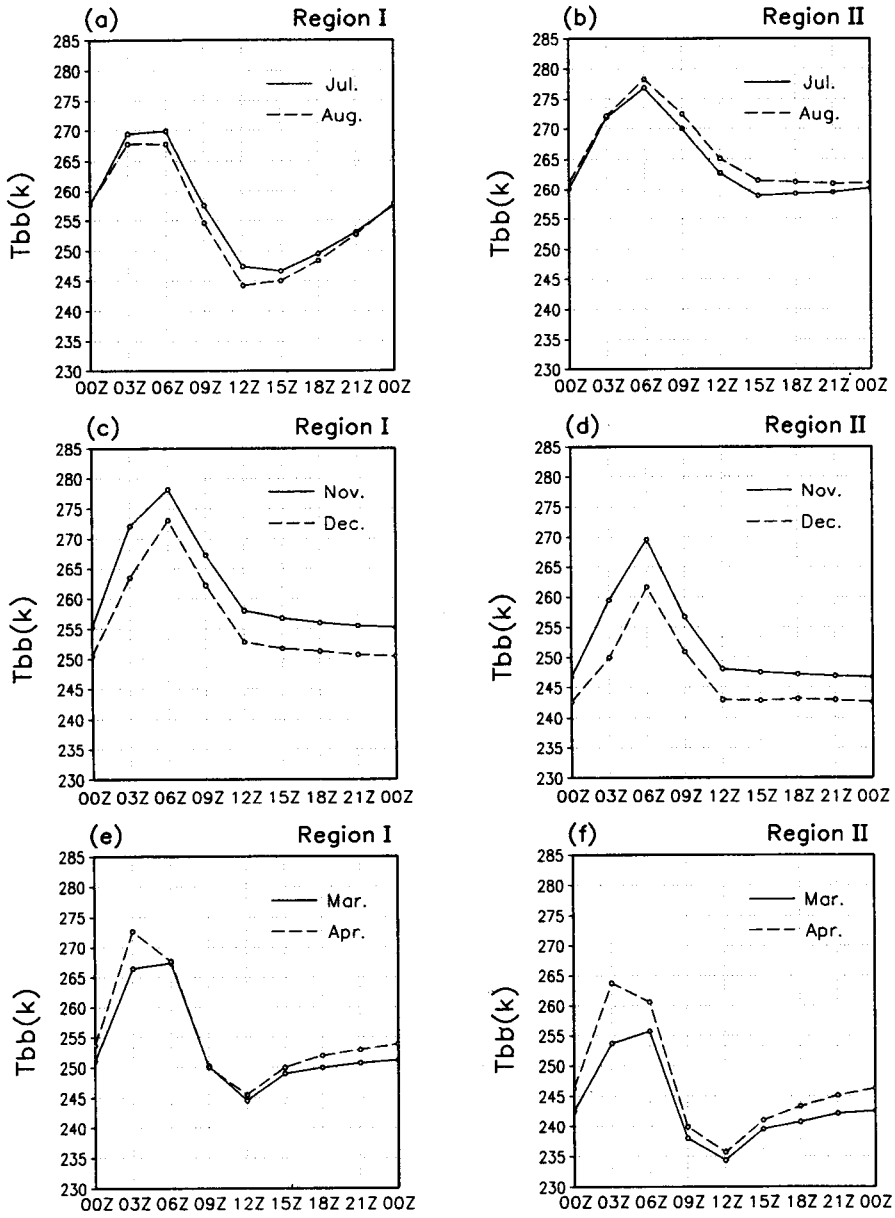

Fig. 2. 6-year (1989–1994) averaged monthly mean diurnal cycles of Tbb over Region I (left panels) and Region II (right panels) for (a) (b) July, August, (c) (d) November, December and (e) (f) March, April.

during the summer (Murakami 1983; Yanai and Li 1994). Shimizu et al. (2001) showed that precipitation with high storm height developed in the afternoon (12 to 18 UTC) during GAME-Tibet IOP. Considering these results, the minimum value of Tbb in the evening indicates the changes of cloud-top temperature related to cloud development.

Figure 2-b shows the same as Fig. 2-a, but for Region II. Large differences in the diurnal pattern are identified between Region I and Region II. Tbb in Region II rises from the morning and reaches its maximum around 06 UTC (12 LST), and falls again after local noon until 15 UTC (21 LST). Tbb remains near the same value from 15 UTC (21 LST)

through 00 UTC (06 LST). It is well known that frozen ground is broadly distributed over the plateau. So, it is likely that this diurnal cycle represents the ground surface temperature of frozen soil. The ground surface temperature rises after sunrise, and reaches its maximum after local noon. It then falls as incoming solar radiation decreases. After sunset, ground surface temperature continues to fall before sunrise mainly because of radiative cooling. The less pronounced peak around local noon seen in summer of Region I (Fig. 2-a) compared to that in Region II (Fig. 2-b) suggests that convective clouds already start to develop in the late morning over the southern plateau. The diurnal cycles of Tbb for winter months (November, December) are shown in Figs. 2-c and 2-d in Region I and II, respectively. In these winter months, little precipitation is observed over the plateau. The remarkable difference of the diurnal cycle can be found between summer and winter in Region I. In winter, the minimum value does not appear at around 12 UTC (18 LST). The diurnal cycles of the two regions are similar to that of Region II for summer (Fig. 2-b), and most likely represent changes of the surface temperature of frozen soil or snow surface. Spring months (March, April) are shown in Figs. 2-e and 2-f. Diurnal cycles of Tbb are also pronounced and are very similar to that shown in Fig. 2-a. Tbb attains its maximum around 03 to 06 UTC (09–12 LST) and reaches its minimum at 12 UTC (18 LST). Considering the diurnal cycle of the ground surface temperature, it is difficult to believe that the ground surface temperature in the evening is lower than that in the early morning before sunrise. If the diurnal cycle shows that of ground surface temperature, the minimum value must be observed in the morning before sunrise as shown during the winter season (Figs. 2-c, 2-d). So, the minimum value at 12 UTC (18 LST) is considered to reflect changes of cloud-top temperature, which are associated with cloud developments (as shown for the summer monsoon season in Fig. 2-a). After 12 UTC (18 LST), Tbb in Figs. 2-e and 2-f rise more quickly than that in Fig. 2-a, suggesting that the DCAs in summer tend to continue until later at night than those in spring. It is noteworthy that, as in summer monsoon season, cloud activity with diurnal variation appears in spring as well. The role of diurnal convective activity and cloudiness in spring in the seasonal migration of the plateau atmosphere has not been studied, in spite of their potential importance for radiation and energy processes over the plateau.

As mentioned above, it was shown by 3-hourly IR-data that the cloud activity reaches its daily maximum around 12 UTC (18 LST) throughout the year. Moreover, nearly identical diurnal variation was observed over the other plateau regions (not shown). It is important to note that two patterns of diurnal cycles of Tbb can be identified as shown in Figs. 2-a and 2-c. These indicate cloud developments in the evening and the change of the ground surface temperature in the absence of diurnal clouds, respectively. To examine more clearly the characteristics of this diurnal component of cloud activity, we apply the index *Icd* (Index of Cloud activity with Diurnal variation) at each grid point defined by

$$Icd = \mathrm{Tbb}(00\,\mathrm{UTC}) - \mathrm{Tbb}(12\,\mathrm{UTC}), \quad (\mathrm{Tbb}(00\,\mathrm{UTC}) - \mathrm{Tbb}(12\,\mathrm{UTC}) > 0), \quad (3)$$

$$Icd = 0, \quad (\mathrm{Tbb}(00\,\mathrm{UTC}) - \mathrm{Tbb}(12\,\mathrm{UTC}) \leq 0). \quad (4)$$

That is, if the diurnal cycle shows a pattern of cloud development with its peak in the evening, Tbb(12 UTC) becomes lower than Tbb(00 UTC) as shown in Fig. 2-a. Therefore, the daily diurnal amplitude of cloud activity in each grid is determined by Eq.(3). On the other hand, if Tbb represents the ground surface temperature changes as shown in Fig. 2-c, Eq.(4) is adopted. Because Tbb(12 UTC) can not decrease below Tbb(00 UTC). The large value of *Icd* indicates the enhanced diurnal variation of cloud activity. To reveal the seasonal changes of the DCA, we use pentad (5-day mean) *Icd* data for the period of 1989–1994 in this study.

GMS–Visible images with higher spatial resolution of $0.05° \times 0.05°$ and Tbb–IR data with $0.25° \times 0.25°$ are also used to illustrate a process of cloud formation with an apparent diurnal cycle. We present the images on 17 April and 8 July 1996 as examples for spring and summer, respectively. In order to ascertain whether the cloud activities on 17 April and 8 July 1996 are precipitable or not, we use the global surface summary of day data (GLOBALSOD) produced by NOAA/NCDC, including daily mean temperature, wind speed, precipitation and so on for many stations around the world. 40 stations are available over the plateau, though most of the stations are in the eastern part of the plateau (see Fig. 7-a). To examine the circulation field over the plateau and surrounding re-

gion, the 5-day mean NCEP/NCAR reanalysis data on 2.5° × 2.5° are used for the period of 1989–1994.

3. Seasonal variation of the DCA

3.1 Seasonal variation of the DCA over Region I and Region II

Figure 3 shows the time series of 6-year averaged 5-day mean *Icd* in Region I (southern region) and II (western region) as shown in Fig. 1. In Region I (Fig. 3-a), the prominent feature is that the variability of the DCA shows distinct bimodal variance maxima, one from February to May and the other from June to September. *Icd* begins to increase from late January and reaches a maximum value more than 12 in March and April. During the period from late May to early June, *Icd* decreases temporally, indicating that the DCA is suppressed. *Icd* becomes large again from mid-June, and the active DCA persists until mid-September. In Region II (Fig. 3-b), *Icd* becomes large from late January and increases from March to mid-May as in Region I. After early June, the *Icd* value in this region is smaller than that of Region I, indicating that the DCA in spring is more prominent than that in summer in the western region. After mid-September, active DCA can not be identified over either region.

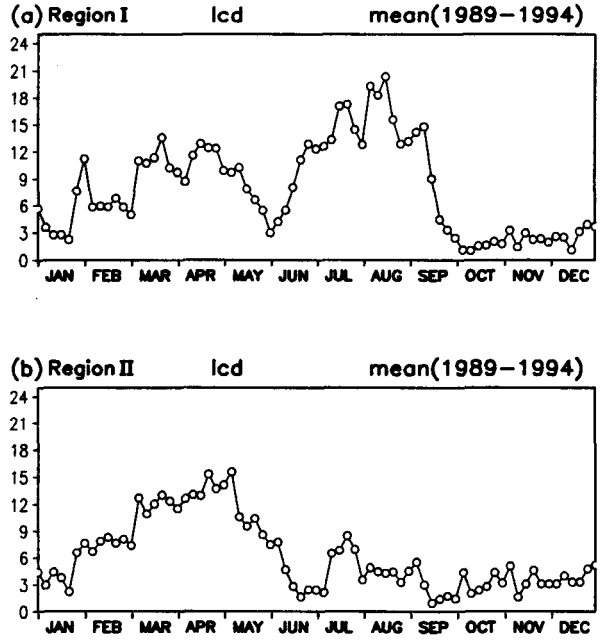

Fig. 3. Time series of 6-year averaged 5-day mean *Icd* for (a) Region I and (b) Region II.

3.2 Horizontal distributions of the DCA

To examine the horizontal distributions of DCA, the 6-year averaged monthly mean *Icd* over the Plateau are produced from January to September, as shown in Fig. 4. In January (Fig. 4-a), no dominant DCA can be identified over the plateau. The DCA starts to appear over almost the whole of the plateau in February (Fig. 4-b). From March to April (Figs. 4-c, 4-d), the enhanced DCA with *Icd* values greater than 10 extends over the whole plateau. The region of the high *Icd* can be found over the zonally-oriented region from 35°N, 80°E to 31°N, 102°E, and around 30°N, 90°E. In May (Fig. 4-e), the DCA persists over the east-west oriented region of central Tibet. The drastic change of the spatial distribution occurs in June (Fig. 4-f); a center of DCA appears over the southeastern region of the plateau centered around 30°N, 101°E. In July, the large *Icd* regions extend from the southern periphery of the plateau to around 35°N with convection center around 30°N, 87°E and 30°N, 100°E. This spatial distribution pattern is in good agreement with that for July shown in Nitta and Sekine (1994), although they used a different cloud activity index (*Ic*). In August, the high DCA persists with a similar pattern until July, but is more active to the west of 95°E. The most enhanced cloud activity appears around 30°N, 86°E. The high DCA extend westward from June to August. The DCA becomes weak and retreats eastward in September (Fig. 4-i). After October, the notable DCA does not appear over the plateau (not shown).

To describe the meridional structure of the DCA more in detail, the latitude-time section of 6-year averaged 5-day mean *Icd* averaged over the same longitude of Region I is indicated in Fig. 5. It should be noted that the meridional seasonal progress of the DCA is quite different between spring and summer. The DCA are slightly enhanced between 28° and 38°N around late January. The high *Icd* area more than 10 can be found from early March to early May. The strong DCA tends to persist until late spring to the north of the central plateau. The suppressed DCA appears from mid-May to early June extending over 27° to 32°N. In the summer monsoon season, the DCA becomes active around 30°N and reaches maximum from July to August, and the high DCA tends to extend over the region to the south of 32°N. Similar seasonal variation of the DCA can be seen over the eastern part of the plateau from 95° to 102°E (not

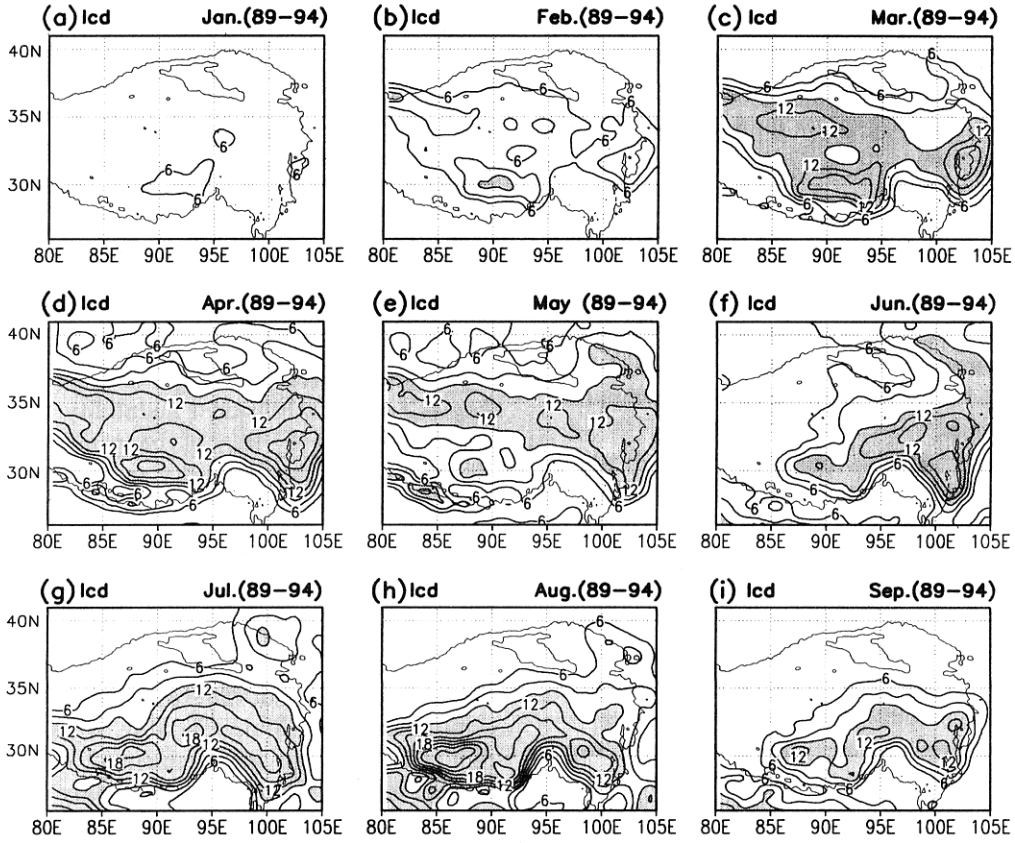

Fig. 4. Horizontal distributions of *Icd* in (a) January, (b) February, (c) March, (d) April, (e) May, (f) June, (g) July, (h) August and (i) September. Shading denotes areas with *Icd* more than 10.

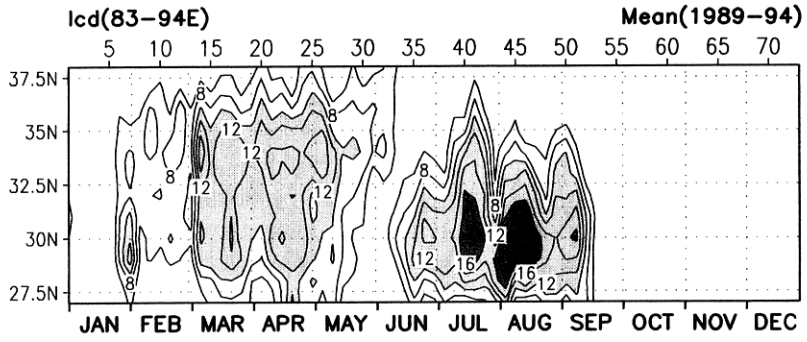

Fig. 5. Latitude-time section of 6-year averaged 5-day mean *Icd* averaged between 83°–93°E. Heavy shading denotes areas with *Icd* greater than 16, while light shading is for areas between 10 and 16.

shown). However, the period of the high DCA in the summer is longer than that to the west of 93°E, corresponding to the early beginning of the DCA in June and the late retreat in September seen in Figs. 4-f and 4-i, respectively. As seen in Figs. 4 and 5, the profound two variance maxima of the DCA are observed, especially, to the south of the central plateau.

3.3 The stability change in the lower atmosphere

It is obvious from Fig. 4 that the center of the lively DCA appears in both spring and summer around Region I. Then, we treat Region I as a key region to study the fluctuation of the DCA and the associated features of atmospheric circulation for both seasons.

The development of convective-type clouds is closely associated with the vertical stability of the atmosphere. The dry and moist static stabilities of the lower atmosphere are especially important factors for controlling convection. In order to clarify the seasonal march of the lower atmospheric stability, we show the vertical gradient of both potential temperature (θ) and equivalent potential temperature (θ_e) between 500 hPa and 400 hPa.

Figure 6 shows the time series of 6-year averaged 5-day mean lower atmospheric stability for both dry and moist convection at 12 UTC (18 LST) over Region I. For dry convection, the low stability with more than -4 K/100 hPa appears from early March to mid-June with a peak in mid-April (-2 K/100 hPa). The stratification from mid-June to mid-September is more stable for dry convection than that from March to early May. The vertical gradient of equivalent potential temperature shows unstable stratification for moist convection after early March. The most unstable conditions for moist convection appear from mid-July to mid-August over the plateau. The two peaks of the DCA in spring and summer, shown in Fig. 3-a, are concurrent with the peaks of the low stability for dry convection and the instability for moist convection, respectively. This result indicates that the enhanced DCAs are induced by different mechanisms in the two seasons.

The lower atmosphere from June to September, during the second *Icd* maximum, is very suitable for deep cumulus convection. However, this observed conditional instability in summer does not imply that convection will occur spontaneously. The release of conditional instability requires the forced lifting to the level of free convection (LFC). The mean relative humidity in the lower troposphere over the plateau is below 100%, even in the boundary layer. Therefore, low-level moisture convergence or strong positive buoyancy is required to induce moist convection. Over the plateau, strong surface heating in daytime can produce positive buoyancy due to the complex terrain surface.

On the other hand, the stratification of the lower atmosphere from March to May, which is concurrent with the first enhancement of *Icd*, is nearly neutral for dry convection and weakly unstable for moist convection. The nearly neutral condition of θ over the lower atmosphere provides a good environment for rising parcels produced by surface heating, because of the decrease of convective inhibition (CIN). Thus, though this condition is not favorable for deep cumulus convection, shallow convection with cumulus-type clouds is highly probable. The DCA is weakened from mid-May to early June

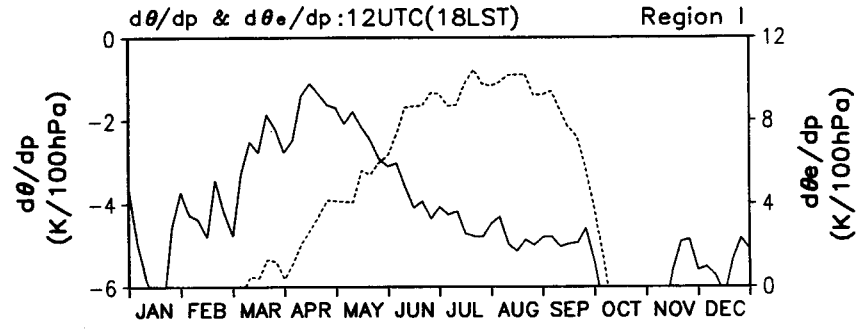

Fig. 6. Time series of 6-year averaged 5-day mean vertical gradient of potential temperature (solid line), and equivalent potential temperature (dashed line with) between 500 hPa and 400 hPa at 12 UTC (18 LST) over Region I. Note that the position of 0 on right axis ($d\theta_e/dp$) is different from that on left axis ($d\theta/dp$).

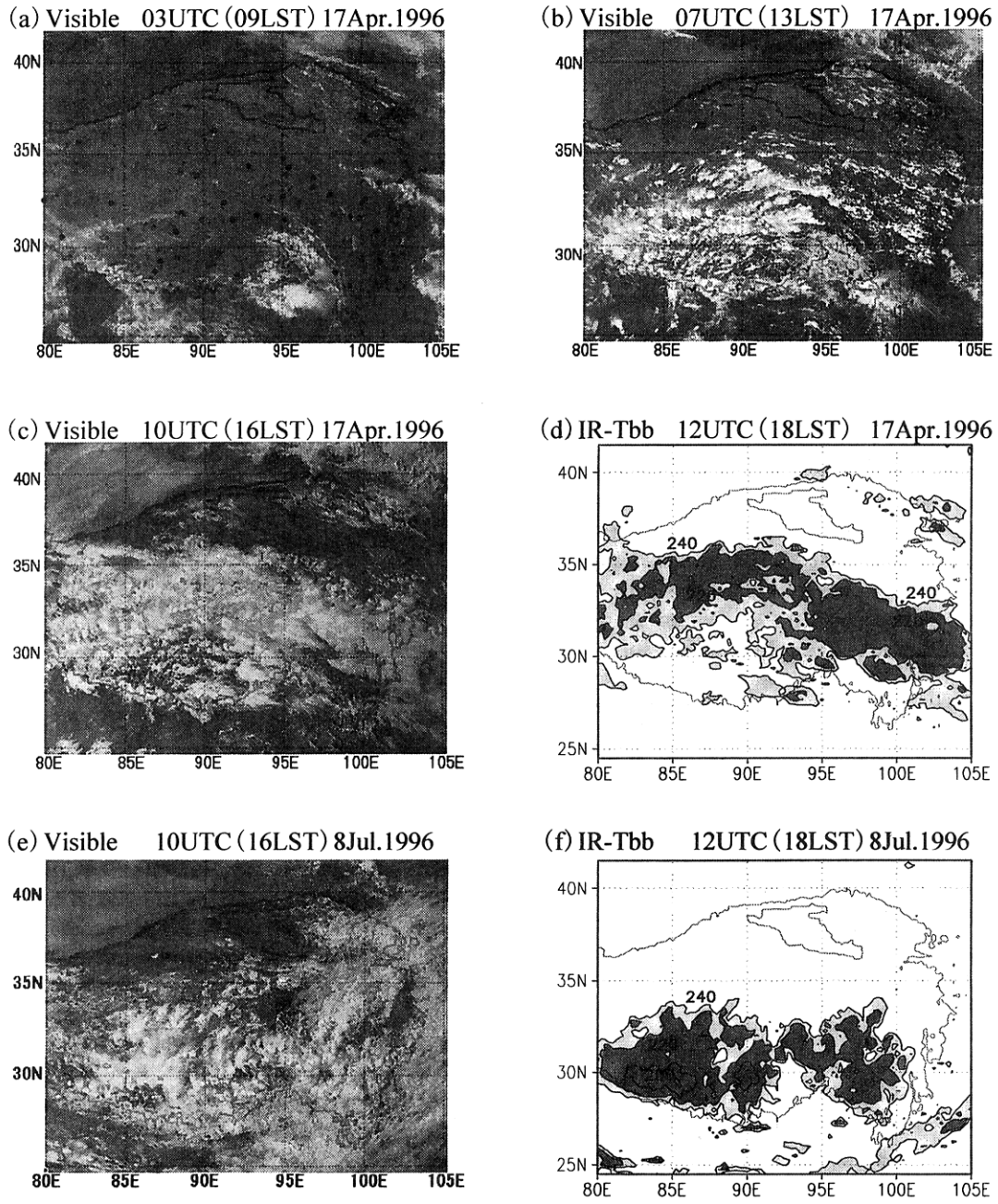

Fig. 7. Visible images of GMS at (a) 03 UTC(09 LST), (b) 07 UTC(13 LST), (c) 10 UTC(16 LST) and (d) the distribution of Tbb (< 240 K) at 12 UTC (18 LST) on 17 April 1996. (e) and (f), same as (c) and (d) but for 8 July 1996. Contour interval is (d), (f) 20 K. The black dots indicate location of surface observation stations for a case study of precipitation in (a). Heavy shading denotes areas with Tbb less than 220 K, while light shading is for areas between 240 to 220 K in (d) and (f).

temporarily as shown in Fig. 3-a. In this transition period, the stratification becomes more stable for dry convection than that from March to April and, is more stable for moist convection than that for summer monsoon season.

3.4 Characteristics of clouds in spring and summer

We have already demonstrated by 6-year averaged *Icd* that the DCA over the plateau has two variance maxima in spring and summer. The DCA for both seasons shows the different characteristics in its spatial distributions and the lower atmospheric stability. In the Asian summer monsoon, active cumulus convection with precipitation is observed over the plateau from the in-situ observations. Therefore, the DCA deduced from *Icd* from June to September represents organized active cumulus convection induced by strong surface heating. On the other hand, the peak of the cloud activity in spring season also appears in the evening. This result suggests that the DCA in spring season also has the properties of convective-type clouds induced by surface heating in daytime. In order to verify the nature of clouds in spring specifically, we examine GMS–Visible images with higher spatial resolution of 0.05° × 0.05° and IR–Tbb data with 0.25° × 0.25°.

Figure 7 shows the images of the cloud developments on 17 April 1996 as an example of a remarkable DCA in spring season. For the comparison of cloud type, images on 8 July 1996 are also shown. At 03 UTC (09 LST) on April 17 (Fig. 7-a), the ground surface of the Tibetan Plateau can be seen with low albedo, indicating fine weather over the plateau. At 07 UTC (13 LST), many convective-type clouds are developing over the plateau. The clouds grow and combine to extend across the plateau area at 10 UTC (16 LST). To the east of 95°E, the convective-type clouds seem to develop into organized cells with stratiform-type clouds. The zonally-oriented distribution of the clouds at this time is quite similar to the *Icd* distribution for April shown in Fig. 4-d. We found that these cloud activities reached their maxima at 12 UTC (Fig. 7-d), and existed until mid-night by 3-hourly GMS–Tbb data (not shown). The cloud top temperature is less than 220 K. If the clouds are blackbody and their top temperature are roughly equivalent to the environmental air temperature observed by NCEP/NCAR reanalysis data, their top height corresponds to about 11000 m above sea level. In spite of the broad existence of the clouds with low Tbb, precipitation is observed on only one station at Xigaze (29.2°N, 88.5°E) on this day, and its value is 1mm per day. As for the synoptic-scale circulation on this day, the westerly jet splits to the southward and the northward of the plateau (not shown). Associated with this circulation field, weak synoptic-scale wind is observed over the plateau. Further studies of the atmospheric structure related to the variability of the DCA in both spring and summer will be presented in Section 4.

In contrast, Fig. 7-e shows the cloud distributions at 10 UTC (16 LST) on 8 July 1996. Convective clouds appear over the plateau to the south of 34°N, especially along 30°N, which is in good agreement with the *Icd* distribution for July (Fig. 4-g). Most of the cloud area attains more than 13000 m above sea level, and the lowest Tbb area around 30°N, 84°E reaches more than 16000 m. As for the synoptic weather condition, the Tibetan high appears over the plateau centered on 31°N, 91°E (not shown). Precipitation is observed at the most stations over the southern part of the plateau. For example, daily precipitation is 6 mm at Xigaze. These images show that the DCA in spring has the nature of convective-type clouds as in summer, although precipitation related to the DCA was observed at more stations in summer than in spring. Considering the stability of the lower atmosphere in spring as shown in Fig. 6, it is probable that the convective-type clouds in spring have higher cloud-base height and shallower cloud-thickness than those in summer. However, further studies are needed to clarify statistically theses cloud properties as well as precipitation, and this will require more detailed and reliable data sets.

4. Atmospheric circulation

In this section, we show the intraseasonal time scales variability of the DCAs and their associated atmospheric circulation fields for both active and inactive periods in the spring and summer monsoon seasons. In this paper, we refer to variations with periodicity from 10 to 90 days as having intraseasonal time scales.

4.1 Intra-seasonal variability of the DCA in spring and summer

Figure 8 shows that the time series of the pentad mean Tbb in Region I at 00 UTC (06 LST), 06 UTC (12 LST) and 12 UTC (18 LST) for each year (1989–1994) from top to bottom. According to the definition of *Icd* mentioned in Section 2, the DCA is active for the period when the Tbb value

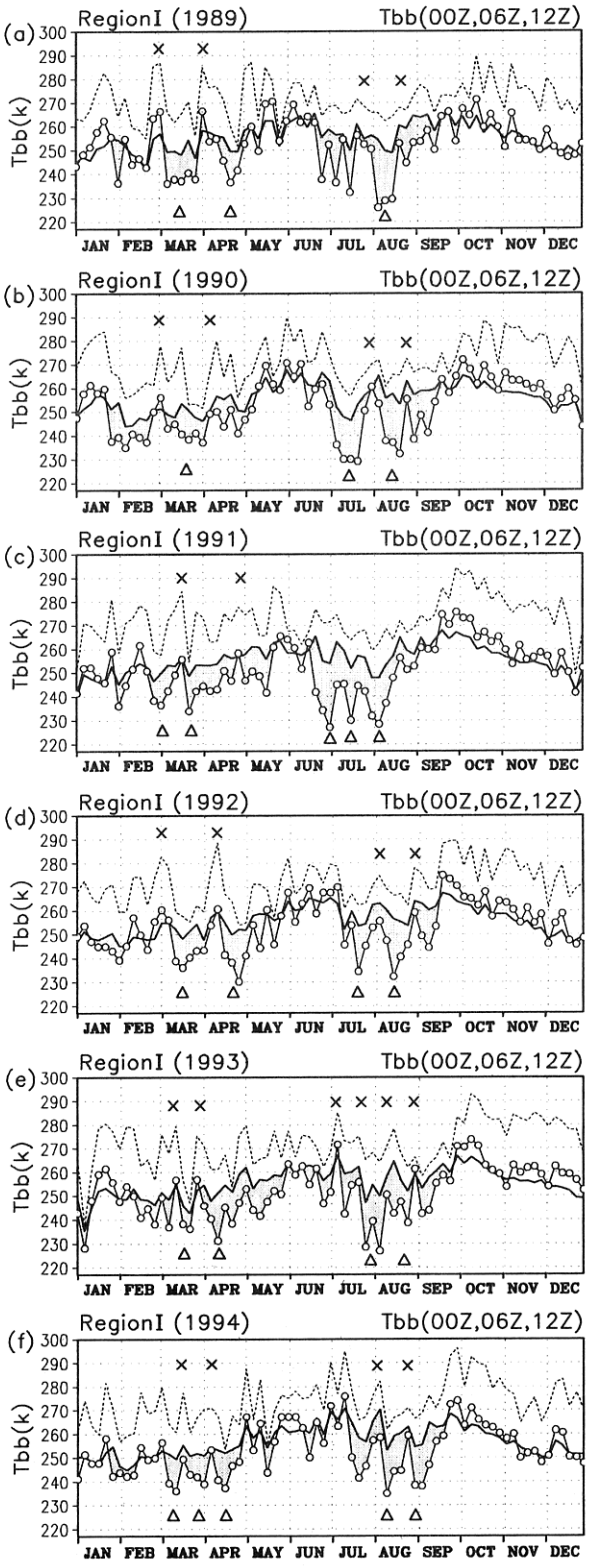

Fig. 8. Time series of 5-day mean Tbb at 00 UTC (06 LST: solid line), 06 UTC (12 LST: dashed line) and 12 UTC (18 LST: solid line with open circle) over Region I :(a) 1989, (b) 1990, (c) 1991, (d) 1992, (e) 1993 and (f) 1994. Shaded periods indicate the active DCA. Triangles and cross marks denote major active and inactive periods of the DCA, respectively.

at 12 UTC (18 LST) is lower than that at 00 UTC (06 LST). So, the shaded period seen in Fig. 8 denotes the enhanced period of the DCA. In each year, the active periods of the DCA can be seen from February to May, and from June to September as shown in the previous section. Moreover, a gap (or break) between the two lively DCA periods is clearly seen in mid-May to early June. A notable feature is that the DCA from February to May show variations on intraseasonal time scales with periodicity of about 15 days and about 30 days, even using the simple pentad mean data. The DCA persists until late April in 1989, 1990, 1992 and 1994 (Figs. 8-a, b, d, f), while the active DCA can be seen even until mid-May in 1991 and 1993 (Figs. 8-b, e). The beginnings of the cloud activity around mid-June correspond to the arrivals of the summer monsoon season over this region. Abrupt transitions are recognized in 1989 and 1991, while gradual transitions are seen in the other years. The DCA from June to September also has a distinct intraseasonal time scales variability.

4.2 The structure of circulation field

In the previous subsection, we showed the marked variability on intraseasonal time scales for the DCAs in both spring and summer. This result suggests that the seasonal variation of the DCA shown in Fig. 3-a is composed mainly of the intraseasonal variability for both seasons. However, considering the differences of the seasonal migration and the spatial distributions in *Icd* (see Fig. 4), we speculate that large differences between spring and summer should exist in the atmospheric circulation related to the DCA variability. To examine the features of atmospheric structure for both active and inactive periods of the DCA, a composite analysis was performed. For understanding how the DCA is enhanced in both seasons, this work is important and useful.

The temporal variations of the DCA in spring and summer were classified into two groups, "ac-

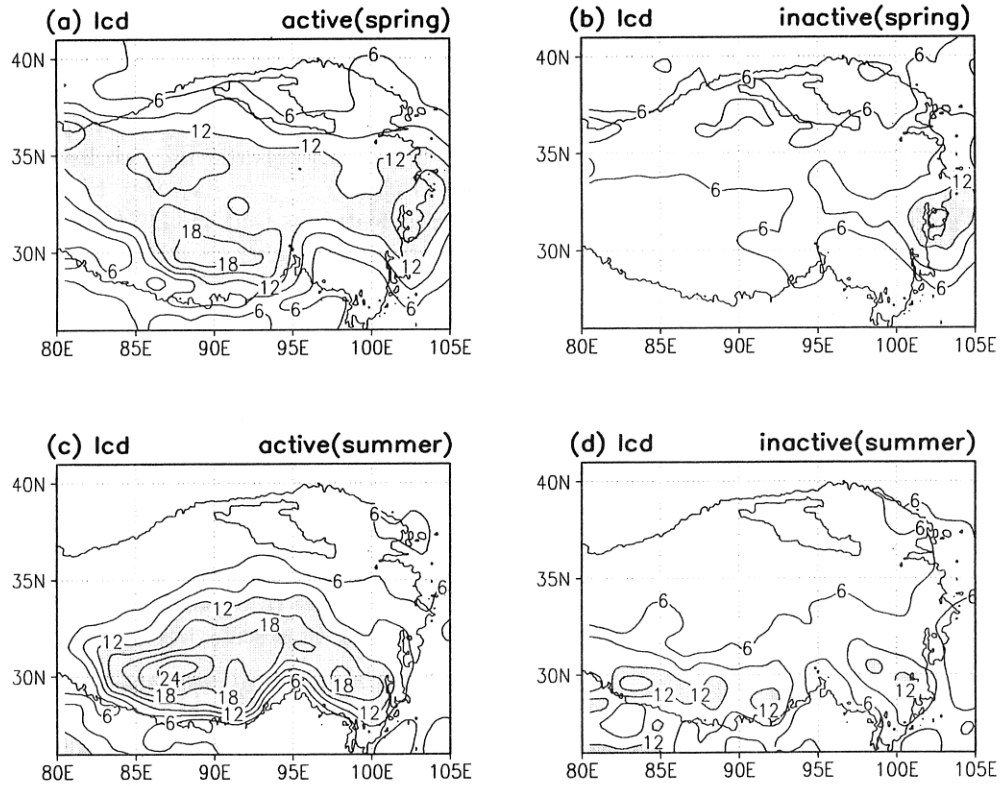

Fig. 9. Composite of *Icd* for (a) active period and (b) inactive period of the DCA in spring. (c) and (d), same as (a) and (b) but for the summer. The contour interval is 3. Shading denotes areas with more than 12.

tive period" and "inactive period" based on Tbb values shown in Fig. 8. In order to show the distinct difference of atmospheric structure, we chose the major active and inactive periods of the DCA between March to April for spring, and July to August for summer. The selected active periods satisfy the following criteria, 1) the period with high DCA (hatched areas in Fig. 8), and 2) the DCA persists for more than two pentad and the period that Tbb (12 UTC) is less than 240 K corresponding to the air temperature near 8000 m in spring (above sea level) and 11000 m in summer over Region I. The definition of inactive period is that Tbb (12 UTC) is more than Tbb (00 UTC) or that Tbb (12 UTC) is larger sufficiently, indicating the suppressed DCA, than that in the active period. Triangle marks and cross marks seen in Fig. 8 denote the selected periods as active and inactive, respectively. Thus, these selected periods represent well the major active and inactive cycle with intraseasonal time scale in the seasons. We did not select the inactive period of summer in 1991, because the DCA is not suppressed sufficiently, compared with the other samples of the inactive period.

Composites of *Icd*, associated with the active and inactive periods of the DCA over region I for both seasons, are shown in Fig. 9. In the active period for spring (Fig. 9-a), the high *Icd* value with more than 12 is observed over the broad extent of the plateau. This distribution of high *Icd* corresponds well to the monthly mean value for March and April seen in Figs. 4-c and 4-d. But for the inactive period (Fig. 9-b), the DCA is suppressed over the plateau to the west of 100°E. Similarly, the *Icd* distribution for active period in summer shows the enhanced DCA to the south of 34°N, which corresponds to the monthly mean for July and August as seen in Fig. 9-c. In the inactive period (Fig. 9-d), the suppressed DCA is found over the plateau clearly, though the relative high *Icd* is observed over the southwestern edge of the plateau.

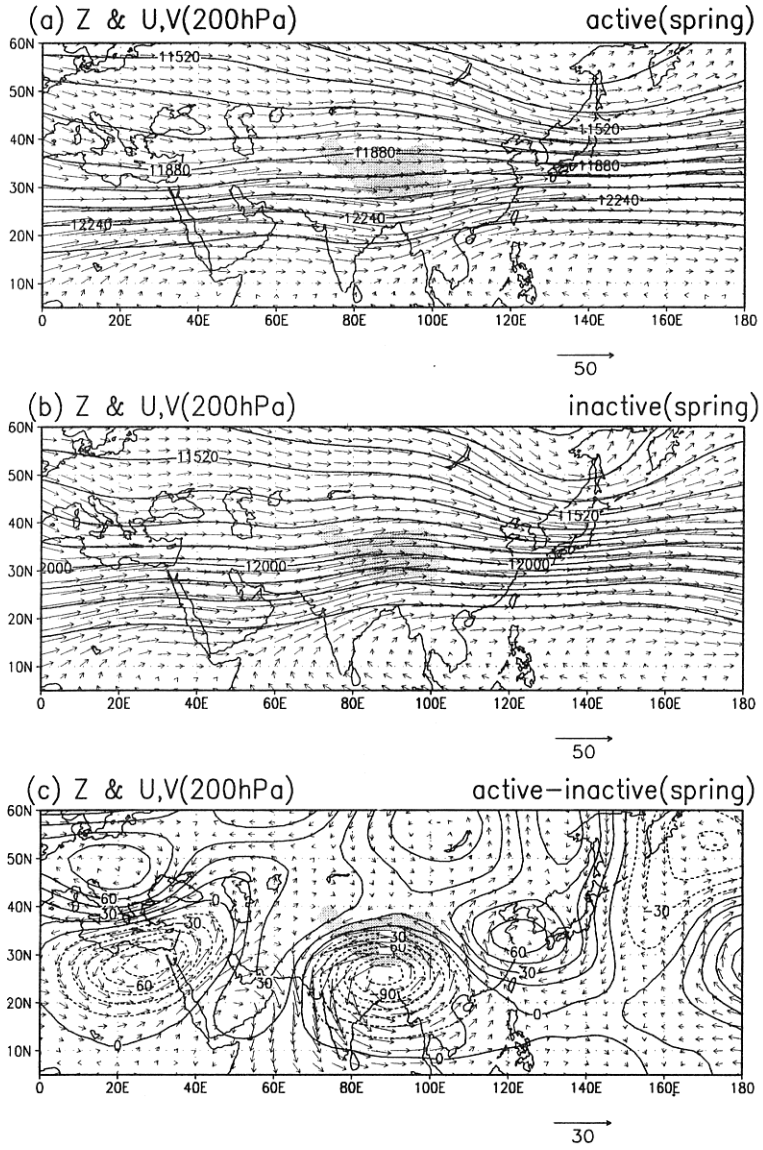

Fig. 10. Composite of geopotential height and wind fields at 200 hPa for (a) active period, (b) inactive period of DCA in spring and (c) difference between the two periods. The contour interval is (a), (b) 60 gpm and (c) 15 gpm. The unit wind vector is (a), (b) 50 ms^{-1} and (c) 30 ms^{-1}. The shaded region indicates the Tibetan Plateau.

The enhanced area of the DCA in spring extends northward compared with that in summer. Thus, we conclude that the variation of *Icd* over Region I is associated well with the plateau scale variation of *Icd*. That is, we regard Region I as a good reference region for the following composite analysis of the atmospheric structure related to the active and inactive periods of the DCA over the Tibetan Plateau.

To examine the difference of circulation fields related to the active and inactive DCAs in spring, the composites of 200 hPa geopotential height and wind fields for (a) active period, (b) inactive period and (c) difference between the two periods are

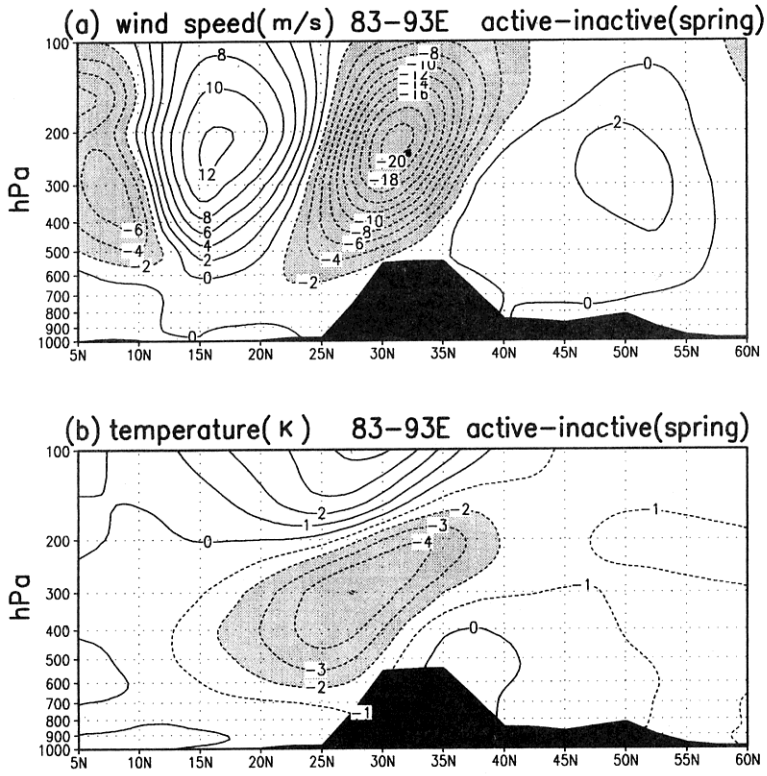

Fig. 11. Latitude-height section of composite difference in (a) windspeed and (b) temperature between active and inactive period of the DCA in spring between 83° and 93°E. The contour interval is (a) $2\,\mathrm{ms}^{-1}$ and (b) 1 K. Shading denotes areas with less than (a) $-2\,\mathrm{ms}^{-1}$ and (b) -2 K.

presented in Fig. 10. Both in Figs. 10-a and 10-b, the prevailing westerly is observed between 0° and 180°E to the north of 10°N. The enhanced DCA period in spring (Fig. 10-a) shows a meandering of the jet stream to the south of the plateau with trough centered around 90°E and the axis of westerly jetstream located around 25°N. It is evident in the inactive period (Fig. 10-b) that the strong jetstream crosses with a shallow ridge over the plateau. The difference (Fig. 10-c) denotes that a large negative anomaly of geopotential height is located over the southern edge of the plateau and another large negative anomaly is observed in the windward side of the plateau around 30°N, 30°E. Note that a wave-type distribution in geopotential anomalies can be found over the subtropical jet. This result suggests that the circulation change over the plateau, which affects the variation of the DCA, is closely associated with that over the upstream region.

Associated with these differences of geopotential height over the plateau and surrounding regions, the windspeed over the plateau varies dramatically. Figure 11-a shows the latitude-height cross section of composite difference in wind speed for the same longitude of Region I. It is obvious from this figure that a large negative anomaly appears over the latitude of the plateau centered around 32°N, 200 hPa. This result indicates that the wind speed is weakened throughout the troposphere over the plateau in the enhanced period of the DCA in spring, and vise versa.

Additionally, the two circulation regimes between active and inactive periods of the DCA in spring are also accompanied by cold and warm temperature anomalies over the plateau, respectively. Figure 11-b shows the same as Fig. 11-a, except the temperature difference. Because the tropospheric temperature increase with seasonal migration in spring, a Fourier analysis was applied to the temperature data to remove the part with frequency

lower than 90 days. Negative temperature anomaly centered at 28°N, 300 hPa can be seen over the plateau. The value of the negative temperature anomaly increases with height and a positive temperature anomaly is also found to the north of 33°N below 400 hPa. These results suggest that the upper-level cold air mass penetrates over the plateau and that the stratification of the troposphere becomes more unstable in the active DCA period. The anomaly sign reverses and the stratification of the troposphere over the plateau become more stable in the inactive DCA period.

Climatologically, the axis of the subtropical jet exists to the south of the plateau in March and April (not shown). Because a cold air mass extends on the northern side of this jet axis related to thermal wind balance, the cold air can easily intrude into the middle and upper troposphere over the plateau during this season. In addition, surface heating increases over the plateau as incoming solar radiation increases in the mid-latitudes in spring. Because of these seasonal backgrounds, the stabil-

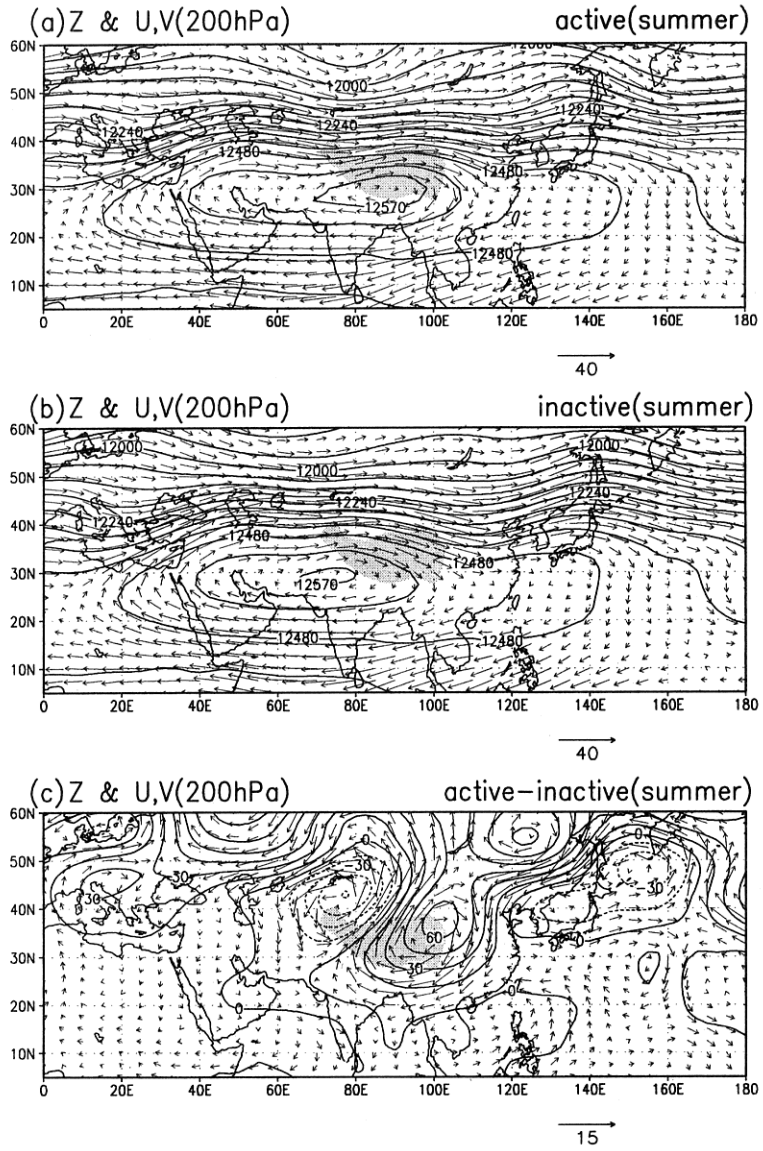

Fig. 12. Same as Fig. 10 except for the summer. The contour interval is (a), (b) 60 gpm and (c) 15 gpm. The unit wind vector is (a), (b) 40 ms^{-1} and (c) 15 ms^{-1}. The contour with 12570 gpm is added to show the center of Tibetan high.

ity for dry convection is more unstable in spring than in the other seasons as shown in Fig. 6. The atmospheric circulation seen in Fig. 10-a is a typical case in which a trough is situated to the south of the plateau and a cold air mass dominates over the whole plateau. Meanwhile, a weak synoptic wind condition over the plateau is likely to induce a thermally driven local circulation due to complex topography of the plateau. This would contribute greatly to development of the convective clouds. Therefore, we conjecture that the destabilization of the troposphere caused by the intrusion of cold air mass in the middle or upper troposphere (relating to the mean features of the upper-level subtropical jet), together with the weak wind speed and the strong surface heating in daytime over the plateau, provide a favorable condition to enhance the DCA in spring.

As mentioned previously, the DCA is weakened from late May to early June over the southern part of the plateau. In this season, the axis of the upper-level subtropical jet shifts northward up to 36°N (not shown), as a result of seasonal warming of the troposphere in the mid-latitudes. This seasonal feature implies that a cold air intrusion, which produces favorable conditions for convection on this region, can not reach the southern part of the plateau easily. In contrast, over the northern part of the plateau, the DCA tends to persist until early June (see Fig. 5) affected by a cold air mass.

Next, we examine the circulation field associated with the DCA in summer. The composites in geopotential height and wind fields at 200 hPa for the (a) active period, (b) inactive period and (c) difference between the both periods are indicated in Fig. 12. It is evident in both Figs. 12-a and 12-b that a large anticyclonic circulation is dominated between 20°E and 150°E with a ridge line along 29°N, and a westerly jet stream appears to the north of the plateau. In the active period of the DCA in summer (Fig. 12-a), the center of the Tibetan high is observed around 29°N, 90°E, which may be related to the enhanced DCA over the southern plateau. Nitta (1983) showed that the heat source, relative vorticity and precipitation change with the period of 10–30 days for the analysis of the eastern plateau, and that the strength of the anticyclonic circulation at the upper troposphere also increases, when the tropospheric heating increases. In the inactive period (Fig. 12-b), the center of the Tibetan high moves westward to 30°N, 70°E and the northeastern edge

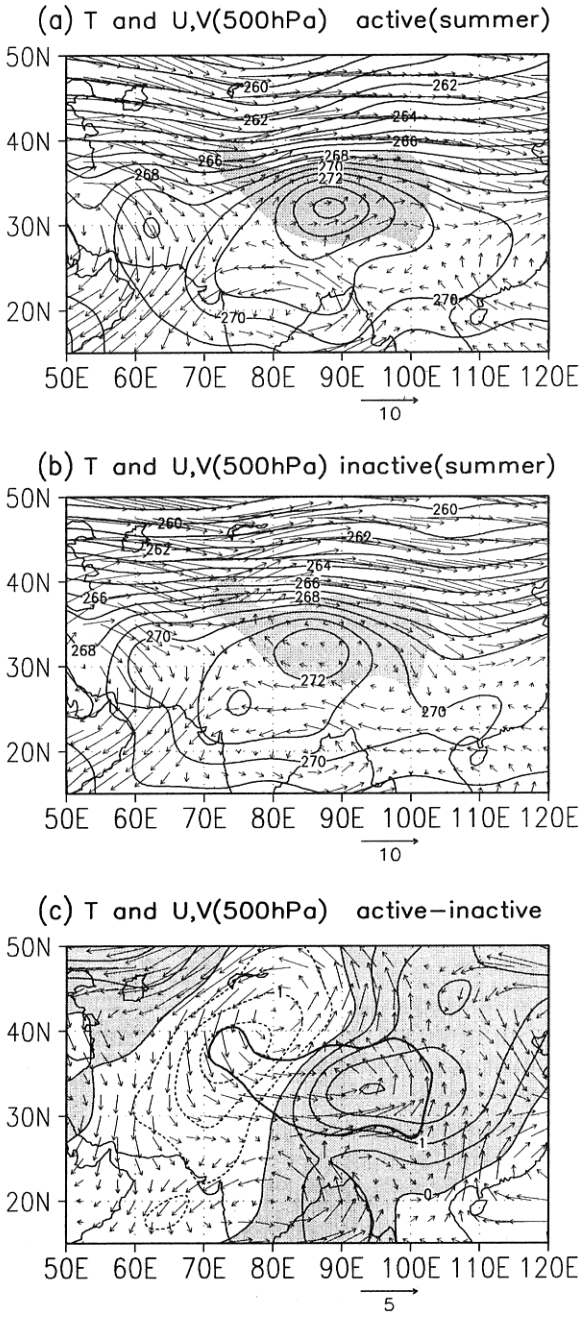

Fig. 13. Composite of temperature and wind fields at 500 hPa for (a) active period, (b) inactive period of the DCA in summer and (c) difference between the two periods. The contour interval is (a), (b) 1 K and (c) 0.5 K. The unit wind vector is (a), (b) 10 ms^{-1} and (c) 5 ms^{-1}. (a), (b) The shading region indicates the Tibetan Plateau. (c) Shading denotes the area of positive anomaly.

of the high covers the plateau. That is, the active/inactive DCA is related to the east-west oscillation of the center of the Tibetan anticyclone on intraseasonal timescales. The distributions of anomalies in the composite difference in summer (Fig. 12-c) around the plateau are quite different from that in spring (Fig. 10-c). Large geopotential anomalies are observed along the northern periphery of the plateau. A positive anomaly is apparent centered around 37°N, 101°E, and a negative anomaly is found centered around 41°N, 78°E, indicating the enhancement of the anticyclonic circulation over the plateau in the active period. This result may suggest an interaction between the active/inactive cycle of the DCA over the plateau and the westerly flow pattern associated with a low frequency mode in summer.

To reveal the difference of temperature and wind fields in the lower atmosphere, the horizontal distributions of these elements at 500 hPa for (a) active period, (b) inactive period and (c) the difference between the two periods are shown in Fig. 13. It is apparent in the active period (Fig. 13-a) that the southerly wind component is dominated over the plateau to the east of 78°E, and a warm center is located around 32°N, 88°E. A branch of the southerly wind toward the southern part of the plateau, which carries a humid and warm air mass, is found from the South Asian monsoon area along 90°E. In contrast, in the inactive period (Fig. 13-b), the southerly wind is not evident over the plateau, and a weak northerly wind spreads to the east of 95°E. The northerly wind becomes more prominent between 400 hPa and 200 hPa over the plateau to the east of 85°E (not shown). The warm center is weakened and moves slightly westward. In the difference of the two periods (Fig. 13-c), a positive temperature anomaly appears over the plateau to the east of 80°E, and a negative anomaly is located around 38°N, 75°E. The positive and negative temperature anomalies over the plateau and surrounding regions are associated roughly with the southerly and northerly wind anomalies, respectively.

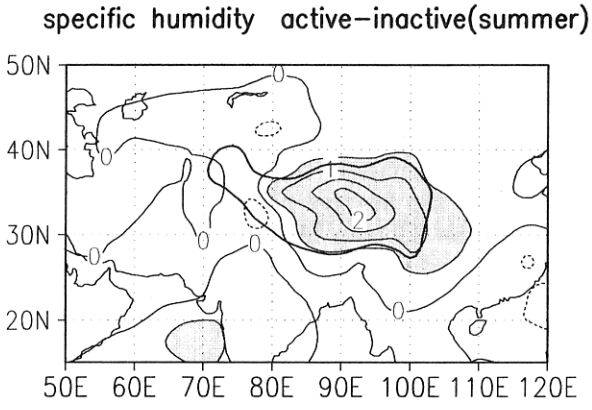

Fig. 14. Composite difference in specific humidity at 500 hPa between active and inactive period of the DCA in summer. The contour interval is 0.5 gKg^{-1}. Shading denotes the area with more then 0.5 gKg^{-1}.

In addition, the two regimes between active and inactive periods of the DCA in summer are also related to the humid and dry anomalies of the lower atmosphere over the plateau. Figure 14 shows the composite difference in specific humidity at 500 hPa. The positive anomaly extends to the east of 80°E over the plateau, which may result in the humid southerly wind and the increase of precipitation in the active period. The increase of air temperature and specific humidity in the lower atmosphere enhances the instability for the moist convection. The atmospheric stratification becomes stable as air temperature and humidity decrease in the lower atmosphere.

These results suggest that a humid and warm air mass intrusion from the South Asian monsoon area into the lower troposphere over the plateau enhances the DCA in summer and, as a result, the Tibetan high is strengthened over the southern part of the plateau. Meanwhile, it is also conceivable that the atmospheric circulation over and surrounding regions in the active period induces the increase of a humid and warm air mass transport into the plateau. It provides a suitable environment for moist convection. In the inactive period, a dry and cold air mass intrusion from the northwest into the plateau prevents a humid and warm air mass transporting from the south. This may be a cause of an increase of stability for moist convection and a suppressed DCA over the plateau, indicating that an air mass intrusion from the north affects the convective activity over the plateau through different processes from those in spring. Thus, we conjecture that the existence of the Tibetan high, the increase of air temperature and specific humidity in the lower atmosphere, and also the strength of heating from the surface in daytime are closely related to the enhanced DCA in summer. To understand detailed processes of the DCA variability, a further study for a transition period between in-

active and active (active and inactive) periods is needed.

Intensive surface and aerological observations was conducted in the Tanggula mountain area (33°N, 92°E) in the central plateau under CREQ (Cryosphere research on Qinzang Plateau) project from May to September in 1993. These observations revealed that the quasi-biweekly fluctuation in surface meteorological elements dominates after the onset of the summer monsoon season over the plateau. It is also reported that the remarkable increase of moisture was observed in the southerly wind, while rapid decrease of moisture through the troposphere occurred periodically associated with cold and dry northerly wind and fair weather (Endo et al. 1994). These findings from the in-situ observations support our results concerning the circulation changes associated with the active/inactive cycle of the DCA in summer.

5. Summary and remarks

In this paper, we examined the seasonal and spatial distributions of the DCA over the Tibetan Plateau throughout the year using index *Icd*, which represents the diurnal amplitude of cloud activity. The DCA is active in spring, as well as in the summer monsoon season. Remarkable differences in seasonal march and spatial distribution of the DCA are found between the two seasons. In addition, intraseasonal variability of the DCA is clearly seen for both seasons. The features of atmospheric circulation associated with active/inactive periods of the DCA are also examined. These results are summarized as follows.

1) The variability of the DCA shows two distinct variance maxima: One in spring, and the other in the summer monsoon season. The DCA begins in late January over the broad extent of the plateau, and reaches its annual maximum from March through April. The DCA extends over almost the whole plateau, with nearly complete coverage over the southern part around 30°N, 90°E and along a zonally oriented belt between 35°N, 80°E and 31°N, 102°E. A short break between the two enhanced seasons of the DCA is found around late May to early June. The DCA intensifies again over the southeastern region of the plateau centered around 30°N, 101°E in June. From July to August, the DCA reaches its second annual maximum, and the most active region appears over the southern region around 30°N, 86°E. After September, the active area of the DCA retreats to the southeastern region.

2) The peak of the DCA in spring shows low stability for dry convection and weak instability for moist convection in the lower atmosphere. Though this stratification is not favorable for deep convections, shallow convection with convective-type clouds is highly probable. The second peak of the DCA in summer is associated with the moist instability, which is suitable for deep cumulus convection.

3) As an example of remarkable DCA in spring and summer, the cloud developments on 17 April 1996 and 8 July 1996 are illustrated using GMS–Visible and IR–Tbb images with higher spatial resolution. The cloud on 17 April 1996 shows the properties of a convective-type cloud, with cloud-top height reaching more than 11000 m above sea level. Precipitation is not observed at most stations. On 8 July 1996, well-organized cumulus convection with precipitation can be seen over the southern part of the plateau. The highest cloud height reaches more than 16000 m above sea level.

4) The DCAs in both spring and summer change with intraseasonal time scales with periodicities of about 15 days and about 30 days. In spring, the enhanced DCA period is associated with a meandering of the jetstream over the plateau with a trough over and to the south of the plateau, while the suppressed DCA period corresponds to the jetstream crossing over the plateau with a shallow ridge. The enhanced (suppressed) DCA are associated well with a weak (strong) wind speed through the troposphere over the plateau, and the cold (warm) air mass in the upper atmosphere over the plateau. In the active DCA period in summer, the center of the Tibetan high is located over the southern part of the plateau where enhanced diurnal convection occurs associated with the warm and humid air mass in the lower atmosphere. In contrast, in the inactive period of the DCA, the center of the Tibetan high shifts westward, and northerly wind with a cold and dry air mass dominates across the plateau throughout the troposphere.

This study confirmed that the DCA is pronounced not only in summer, but also in spring. The DCA is modulated with intraseasonal time scales in both seasons. Intraseasonal modulations with the periodicities of about two weeks and 30–60 days in wind fields, cloudiness and the other meteorological elements are prominent phenomena over the Tropics and the Asian monsoon region

(Madden and Julian 1972; Yasunari 1979; Murakami 1984; Krishnamurti and Gadgil 1985; Nakazawa 1991). These disturbances are of convective origin and these scales are of zonal wavenumber 1 to 3.

Nitta (1983) found from a case study for 1979 that intraseasonal variations with the periods of 10–15 and -30 days appear in total heating, precipitation and relative vorticity in the upper troposphere over the eastern plateau during the summer monsoon season. He also showed that a large convective heating is associated with large amounts of precipitation and enhanced upper level anticyclonic circulation with intraseasonal time scales. The variations of precipitation over the plateau and over India are opposite phase. This phenomenon was explained by cloud systems moving northward from the tropics to the southern foothills of the Himalayas with intraseasonal variation (Yasunari 1979, 1980, 1981). In this study, the DCA over the plateau intensifies on intraseasonal time scales, although the relationship between the time variation of the DCA over the plateau and that of the whole summer monsoon activity is not examined. In the vicinity of the South China Sea, the diurnal cycle of cloud activity over land is suppressed in the disturbed period of intraseasonal variation in the northern summer, because the broad cloud coverage caused by large scale ascending motions reduces the incoming solar radiation (Chen and Takahashi 1995). It is suggested that the response of diurnal variation over the plateau to the intraseasonal variation is different from that over the tropics.

Some studies pointed out that intraseasonal variations are also seen in the extratropics (Krishnamuruti and Gadgil 1985). Waves with wavenumber 5–7 trapped in the subtropical jet on 10- to 30- day time scales were investigated by Blackmon et al. (1984), Hsu and Lin (1992), Kiladis and Weickmann (1992) and Terao (1998) for the northern hemisphere. Terao (1998) showed that standing wave-like disturbances with a 32-day period are found in the subtropical jet during the northern summer, through a case study for a typical year (1983). Their propagation routes correspond to the well-defined wave-guide for the quasi-stationary Rossby wave formed along the subtropical jet. He also noted the 25-day low pass filtered wind velocity vector at 200 hPa and temperature at 300 hPa on the enhanced wave days. It is interesting that the wind fields shown in both Figs. 12-a and 12-b in our study are quite similar to those seen in his analysis for the enhanced wave days (See Fig. 8 in Terao 1998). These results suggest that the intraseasonal variation of the DCA over the plateau in summer monsoon season may be affected by the low-frequency disturbances of both the midlatitude westerly and Asian monsoon regions. Further study is needed to clarify whether heating over and around the plateau forces the westerly, or whether the DCA over the plateau fluctuates in response to the westerly jet.

On the other hand, the DCA in spring also changes with intraseasonal timescales. In spring, the subtropical jet is situated in the lower latitude than that in summer. As seen in Fig. 10-c, a wave-train type distribution of geopotential height anomaly with wavenumber 5–6 appears over the westerly region. It is likely that the variation of the DCA in spring is also related to the disturbances on intraseasonal timescales over the westerly region, although a more detailed study is necessary to capture the characteristics of low-frequency disturbances over the subtropical jet in spring. Since the strong westerly prevails over the same latitude of the Tibetan Plateau in this season, it may be plausible that the dynamical effect of the plateau orography changes depending on the intensity and the meridional position of the upstream jet, which in turn may induce a bimodal response of the circulation over and around the plateau.

The DCA in spring also varies on interannual time scales as shown in Fig. 8. The persistence of the DCA until late spring suggests the delay of the seasonal migration of the atmospheric circulation over the plateau and surrounding region. It would be interesting to examine how the DCA and the structure of atmospheric circulation in spring relate to the onset and activity of the following Asian summer monsoon. Clarifying the role of the spring DCA in the seasonal heating processes over the plateau will require further studies of precipitation, cloud-radiation feedback processes and land-surface heating during this season.

Acknowledgments

The authors express sincere thanks to Dr. Hiroaki Ueda of the Meteorological Research Institute for his thoughtful discussion and comments. They also thank Dr. Kiyotoshi Takahashi of the Meteorological Research Institute, and Dr. Tokio Kikuchi of University of Ko-chi, who provided GMS–IR data and visible images. This work was supported in

part by a Grant-In-Aid from the Scientific Research on Priority Areas (B) (1) (No. 11201101).

References

Blackmon, M.L., Y.-H. Lee and J.M. Wallace, 1984: Horizontal structure of 500 mb height fluctuations with long, intermediate and short time scales. *J. Atmos. Sci.*, **41**, 961–979.

Chen, T.-C. and K. Takahashi, 1995: Diurnal variation of outgoing longwave radiation in the vicinity of the South China Sea: Effect of intraseasonal variation. *Mon. Wea. Rev.*, **123**, 566–577.

Endo, N., 1996: A study on the structure of planetary boundary layer over the Tibetan Plateau, Ph. D. Thesis, University of Tsukuba, 135pp.

———, K. Ueno and T. Yasunari, 1994: Seasonal change of the troposphere in the early summer of 1993 over central Tibet observed in the Tanggula mountains. *Bull. Glacier Res.*, **12**, 25–30.

Gao, Y.-X., M.-C. Tang, S.-W. Luo, Z.-B. Shen and C. Li, 1981: Some aspects of recent research on the Qinghai-Xizang Plateau meteorology. *Bull. Amer. Meteor. Soc.*, **62**, 31–35.

He, H., J.W. McGinnis, Z. Song and M. Yanai, 1987: Onset of the Asian monsoon in 1979 and the effect of the Tibetan Plateau. *Mon. Wea. Rev.*, **115**, 1966–1995.

Hsu, H.-H. and S.-H. Lin, 1992: Global teleconnections in the 250-mb streamfunction field during the northern hemisphere winter. *Mon. Wea. Rev.*, **8**, 1169–1190.

Kiladis, G.N. and K.M. Weickmann, 1992: Circulation anomalies associated with tropical convection during northern winter. *Mon. Wea. Rev.*, **120**, 1900–1923.

Koike, T., T. Yasunari, J. Wang and T. Yao, 1999: GAME–Tibet IOP summary report. *Proceedings of the 1st International Workshop on GAME–Tibet (January 1999, Xi'an China)*. 1–2.

Krishnamurti, T.N. and S. Gadgil, 1985: On the structure of the 30 to 50 day mode over the globe during FGGE. *Tellus.*, **37A**, 336–360.

Li, C. and M. Yanai, 1996: The onset and interannual variability of the Asian summer monsoon in relation to land-sea thermal contrast. *J. Climate*, **9**, 358–375.

Luo, H. and M. Yanai, 1983: The large-scale circulation and heat sources over the Tibetan Plateau and surrounding areas during the early summer of 1979. Part I: Precipitation and Kinematic Analyses. *Mon. Wea. Rev.*, **111**, 922–944.

——— and M. Yanai, 1984: The large-scale circulation and heat sources over the Tibetan Plateau and surrounding areas during the early summer of 1979. Part II: Heat and Moisture budgets. *Mon. Wea. Rev.*, **112**, 966–989.

Madden, R.A. and P.R. Julian, 1972: Description of global-scale circulation cells in the Tropics with a 40–50 day period. *J. Atmos. Sci.*, **29**, 1109–1123.

Murakami, M., 1976: Analysis of monsoon fluctuations over India. *J. Meteor. Soc. Japan*, **54**, 15–31.

———, 1983: Analysis of the deep convective activity over the western Pacific and Southeast Asia. PartI: Diurnal variation. *J. Meteor. Soc. Japan*, **61**, 60–76.

———, 1984: Analysis of the deep convective activity over the western Pacific and Southeast Asia. Part II: Seasonal and intraseasonal variations during northern summer. *J. Meteor. Soc. Japan*, **62**, 88–108.

Murakami, T. and J. Matsumoto, 1994: Summer monsoon over Asian continent and western North Pacific. *J. Meteor. Soc. Japan*, **72**, 719–745.

Nitta, T., 1983: Observational study of heat sources over the eastern Tibetan Plateau during the summer monsoon. *J. Meteor. Soc. Japan*, **61**, 590–605.

——— and S. Sekine, 1994: Diurnal variation of convective activity over the Tropical Western Pacific. *J. Meteor. Soc. Japan*, **72**, 627–640.

Ose, T., 1996: The comparison of the simulated response to the regional snow mass anomalies over Tibet, Eastern Europe, and Siberia. *J. Meteor. Soc. Japan*, **74**, 845–866.

Shi, L. and E.A. Smith, 1992: Surface forcing of the infrared cooling profile over the Tibetan Plateau. Part II: Cooling rate variation over large-plateau domain during summer monsoon tradition. *J. Atmos. Sci.*, **49**, 823–844.

Shimizu, S., K. Ueno, H. Fujii, H. Yamada, R. Shirooka and L. Liu, 2001: Mesoscale characteristics and structures of stratiform precipitation on the Tibetan Plateau. *J. Meteor. Soc. Japan*, **79**, 435–461.

Smith, E.A. and L. Shi, 1995: Reducing discrepancies in atmospheric heat budget of Tibetan Plateau by satellite-based estimates of radiative cooling and cloud-radiation feedback. *Meteorol. Atmos. Phys.*, **56**, 229–260.

Terao, T., 1998: Barotropic disturbances on intraseasonal time scales observed in the midlatitude over the Eurasian Continent during the northern summer. *J. Meteor. Soc. Japan*, **8**, 419–436.

Ueda, H. and T. Yasunari, 1998: Role of warming over the Tibetan Plateau in early onset of the summer monsoon over the Bay of Bengal and the South China Sea. *J. Meteor. Soc. Japan*, **76**, 1–12.

Uyeda, H., H. Yamada, J. Horikomi, R. Shirooka, S. Shimizu, L. Liu, K. Ueno, H. Fujii and T. Koike, 2001: Characteristics of convective clouds observed by a Doppler radar at Naqu on Tibetan Plateau during GAME–Tibet IOP. *J. Meteor. Soc. Japan*, **79**, 463–474.

Vernekar, A.D., J. Zhou and J. Shukla, 1995: The effect of Eurasian snow cover on the Indian monsoon. *J. Climate*, **8**, 248–266.

Yanai, M. and C. Li, 1994: Mechanism of heating and the boundary layer over the Tibetan Plateau. *Mon. Wea. Rev.*, **122**, 305–323.

———, C. Li and Z. Song, 1992: Seasonal heating of the Tibetan Plateau and its effects on the evolution of the Asian summer monsoon. *J. Meteor. Soc. Japan*, **70**, 319–351.

Yasunari, T., 1979: Cloudiness fluctuations associated with the Northern hemisphere summer monsoon. *J. Meteor. Soc. Japan*, **57**, 227–242.

———, 1980: A quasi-stationary appearance of 30 to 40 day period in the cloudiness fluctuations during the summer monsoon over India. *J. Meteor. Soc. Japan*, **58**, 225–229.

———, 1981: Structure of an Indian summer monsoon system with around 40-day period. *J. Meteor. Soc. Japan*, **59**, 336–354.

———, A. Kitoh and T. Tokioka, 1991: Local and remote responses to excessive snow mass over Eurasia appearing in the northern spring and summer climate.—a study with the MRI GCM. *J. Meteor. Soc. Japan*, **69**, 473–487.

Yeh, T.-C. and Y.-X. Gao, 1979: *The meteorology of the Qinghai-Xizang (Tibet) Plateau*, Science Press, Beijing, 278 pp (in Chinese).